



Non-invasive mapping of epileptogenic networks predicts surgical outcome

Ludovica Corona,^{1,2} Eleonora Tamilya,³ M. Scott Perry,¹ Joseph R. Madsen,⁴ Jeffrey Bolton,⁵ Scellig S. D. Stone,⁴ Steve M. Stufflebeam,⁶ Phillip L. Pearl⁵ and Christos Papadelis^{1,2,7}

Epilepsy is increasingly considered a disorder of brain networks. Studying these networks with functional connectivity can help identify hubs that facilitate the spread of epileptiform activity. Surgical resection of these hubs may lead patients who suffer from drug-resistant epilepsy to seizure freedom. Here, we aim to map non-invasively epileptogenic networks, through the virtual implantation of sensors estimated with electric and magnetic source imaging, in patients with drug-resistant epilepsy. We hypothesize that highly connected hubs identified non-invasively with source imaging can predict the epileptogenic zone and the surgical outcome better than spikes localized with conventional source localization methods (dipoles). We retrospectively analysed simultaneous high-density electroencephalography (EEG) and magnetoencephalography data recorded from 37 children and young adults with drug-resistant epilepsy who underwent neurosurgery. Using source imaging, we estimated virtual sensors at locations where intracranial EEG contacts were placed. On data with and without spikes, we computed undirected functional connectivity between sensors/contacts using amplitude envelope correlation and phase locking value for physiologically relevant frequency bands. From each functional connectivity matrix, we generated an undirected network containing the strongest connections within sensors/contacts using the minimum spanning tree. For each sensor/contact, we computed graph centrality measures. We compared functional connectivity and their derived graph centrality of sensors/contacts inside resection for good ($n = 22$, ILAE I) and poor ($n = 15$, ILAE II–VI) outcome patients, tested their ability to predict the epileptogenic zone in good-outcome patients, examined the association between highly connected hubs removal and surgical outcome and performed leave-one-out cross-validation to support their prognostic value. We also compared the predictive values of functional connectivity with those of dipoles. Finally, we tested the reliability of virtual sensor measures via Spearman's correlation with intracranial EEG at population- and patient-level. We observed higher functional connectivity inside than outside resection ($P < 0.05$, Wilcoxon signed-rank test) for good-outcome patients, on data with and without spikes across different bands for intracranial EEG and electric/magnetic source imaging and few differences for poor-outcome patients. These functional connectivity measures were predictive of both the epileptogenic zone and outcome (positive and negative predictive values $\geq 55\%$, validated using leave-one-out cross-validation) outperforming dipoles on spikes. Significant correlations were found between source imaging and intracranial EEG measures ($0.4 \leq \rho \leq 0.9$, $P < 0.05$). Our findings suggest that virtual implantation of sensors through source imaging can non-invasively identify highly connected hubs in patients with drug-resistant epilepsy, even in the absence of frank epileptiform activity. Surgical resection of these hubs predicts outcome better than dipoles.

- 1 Jane and John Justin Institute for Mind Health, Cook Children's Health Care System, Fort Worth, TX 76104, USA
- 2 Department of Bioengineering, University of Texas at Arlington, Arlington, TX 76010, USA
- 3 Fetal-Neonatal Neuroimaging and Developmental Science Center, Boston Children's Hospital, Harvard Medical School, Boston, MA 02115, USA

Received June 15, 2022. Revised November 03, 2022. Accepted November 30, 2022. Advance access publication February 15, 2023

© The Author(s) 2023. Published by Oxford University Press on behalf of the Guarantors of Brain.

This is an Open Access article distributed under the terms of the Creative Commons Attribution-NonCommercial License (<https://creativecommons.org/licenses/by-nc/4.0/>), which permits non-commercial re-use, distribution, and reproduction in any medium, provided the original work is properly cited. For commercial re-use, please contact journals.permissions@oup.com

- 4 Division of Epilepsy Surgery, Department of Neurosurgery, Boston Children's Hospital, Harvard Medical School, Boston, MA 02115, USA
- 5 Division of Epilepsy and Clinical Neurophysiology, Department of Neurology, Boston Children's Hospital, Harvard Medical School, Boston, MA 02115, USA
- 6 Athinoula Martinos Center for Biomedical Imaging, Massachusetts General Hospital, Harvard Medical School, Boston, MA 02129, USA
- 7 School of Medicine, Texas Christian University, Fort Worth, TX 76129, USA

Correspondence to: Christos Papadelis, PhD
 Director of Research Center, Jane and John Justin Institute for Mind Health
 Cook Children's Health Care System
 1500 Cooper St., Fort Worth, TX 76104, USA
 E-mail: christos.papadelis@cookchildrens.org

Keywords: epilepsy; functional connectivity; high-density electroencephalography; magnetoencephalography; source localization

Introduction

Epilepsy is the most frequent chronic neurological condition affecting ~50 million people worldwide including children (0.5–1%) and young adults.^{1,2} Approximately 20–30% of these patients are unable to control their seizures with antiseizure drugs and suffer from drug-resistant epilepsy (DRE).³ Children and young adults with DRE are at increased risk for poor long-term intellectual and psychological outcomes, along with a poor health-related quality of life.^{4–9} For these patients, neurosurgery is the best available treatment because it offers higher rates of seizure freedom and better outcome with respect to behaviour and quality of life compared to antiseizure drug therapy alone.¹⁰ Epilepsy surgery requires the precise delineation of the epileptogenic zone (EZ), the brain area that is indispensable for the generation of seizures.¹¹ Current clinical practice uses the seizure onset zone (SOZ), the brain area where seizures initiate, as an EZ surrogate. Yet, its delineation is often challenging as several stereotyped seizures should be recorded at the expense of considerable human and financial resources. Moreover, the SOZ may not represent the full EZ extent.^{12,13} These SOZ limitations have given renewed interest to the development of interictal biomarkers of epileptogenicity.

Epileptogenic activity is often generated by brain networks¹⁴ and spreads across them, rather than by single sources.¹⁵ Studying these networks with functional connectivity (FC) and its derived graph theory metrics may help identifying highly connected hubs that facilitate the spread of epileptiform activity to the rest of the brain. Surgical resection of these hubs may lead to seizure freedom. Recent intracranial electroencephalography (iEEG) studies have demonstrated high interictal FC within resection, which was associated with favourable outcome.^{16–20} Moreover, FC within resected regions of good-outcome patients has been shown to play a more synchronizing role in the overall network compared to poor-outcome patients, suggesting the existence of pathological hubs in the vicinity of the epileptic focus that may facilitate seizure propagation.^{21,22} Although iEEG can identify the EZ in ~60% of patients,²³ it presents limitations because of its invasiveness.²⁴ Moreover, it has limited spatial resolution because its contacts record activity only in their direct vicinity and are blind to other brain areas. Thus, the actual focus of the EZ may be missed leading to surgical failure.

Non-invasive electrophysiological techniques, which can record interictal activity from the whole brain, could overcome the iEEG limitations. Recent magnetoencephalography (MEG) studies showed that FC measures could identify the EZ in patients with DRE,^{25–27} even from recordings with no frank epileptiform activity. This approach of using FC metrics as epilepsy biomarkers regardless the presence of interictal epileptiform discharges (IEDs) would be highly valuable particularly for the ~10% of patients with DRE who do not show IEDs in their recordings.²⁵ Yet, these studies did not assess whether FC presents any additive value to conventional electric and magnetic source imaging (ESI/MSI).

Here, we aim to map non-invasively the epileptogenic network in children and young adults with DRE undergoing epilepsy surgery by analysing interictal high-density EEG (HD-EEG) and MEG data and assess the prognostic value of resecting the non-invasively localized hubs of this network. We hypothesize that highly connected hubs (i.e. brain areas with high interictal FC) estimated non-invasively through virtual sensors (VSs) with ESI/MSI can predict the EZ and the patient's surgical outcome better than IEDs localized with conventional ESI/MSI methods (i.e. dipoles).

Materials and methods

Cohort

We retrospectively reviewed children and young adults with DRE who underwent epilepsy surgery at Boston Children's Hospital between June 2011 and June 2018. We included patients with: (i) pre-operative HD-EEG and MEG; (ii) long-term monitoring with iEEG; (iii) presurgical MRI, postimplantation CT and post-surgical MRI; and (iv) post-surgical follow-up after ≥ 2 years. Surgical outcomes were established based on follow-up visits by a paediatric epileptologist using the International League Against Epilepsy (ILAE) scale²⁸ and classified as good (ILAE I) or poor outcome (ILAE II–VI). The protocol was approved by our Institutional Review Board.

HD-EEG and MEG recordings

MEG data were recorded using a 306-channel system (VectorView, MEGIN). HD-EEG was recorded simultaneously with a 70-electrode cap (EASYCAP Brain Products). Two extra electrodes covering temporal areas were also placed. Electrodes were placed according to

the 10–10 system.²⁹ The recordings were performed for ~1 h in a supine position. Patients were instructed to rest or sleep during recordings. The sampling rate was ≥ 600 Hz.

Long-term iEEG

Long-term iEEG was performed with subdural grids (2.3 mm diameter and 10 mm inter-contact distance) and/or depth electrodes (6–16 linearly arranged contacts with ~1 mm diameter and ~3–5 mm inter-contact distance; Ad-Tech) using the XLTEK NeuroWorks (Natus Inc). For each patient, the location, number and contacts type were prospectively decided independently from this study. Implanted contacts were kept for an average of 5.6 days, 12.6 h and 25.3 min. Data were acquired with ≥ 500 Hz sampling rate. Paediatric epileptologists reviewed each patient's iEEG and extracted multiple 5–10 min segments with frequent IEDs or segments with no (or minimum) IEDs. Channels with artefacts were excluded from further analysis.

Localization of iEEG contacts

MRI scans were performed before and after surgical resection with standard magnetization-prepared rapid acquisition gradient-echo sequences using a 3 T scanner (TIM TRIO, Siemens AG). After implantation, CT scans ($0.5 \times 0.5 \times 0.5$ mm³) were acquired to document iEEG contacts' locations. We determined these locations by co-registering postimplantation CT with preoperative MRI.³⁰ We defined visually the contacts' locations based on their intensity on the co-registered CT-MRI and mapped them on patient's cortical surface reconstructed from the preoperative MRI.³¹ To account for brain shift that occurs after electrocorticography implantation, we projected subdural electrodes onto this cortical surface and adjusted the depth contacts' locations to compensate this shift.^{32,33}

Virtual sensor reconstruction

To build the forward model, we extracted the cortical surfaces from the preoperative MRI using Freesurfer,³¹ and constructed the realistic head models, as a three-layer (i.e. scalp, inner skull and outer skull) geometric model, using boundary element method (BEM),³⁴ for both HD-EEG and MEG. The source space included the entire brain volume.

To solve the inverse problem, we used the linearly constrained minimum variance (LCMV) beamformer³⁵ for localizing the neural activity of each brain location in source space. We computed the data covariance matrix on artefact-free data portions; the noise covariance matrix was set as an identity matrix.

We used the output of beamformer to reconstruct the activity at VSs locations. We placed the VSs at the same locations where iEEG contacts were implanted during the invasive monitoring enabling a direct comparison between the non-invasively estimated epileptogenic networks and the invasive benchmark [Fig. 1A(i)]. To calculate VSs, we defined non-overlapping regions of interest for each iEEG contact and included the closest volume points surrounding each contact's centre: 5 and 10 mm for depth and subdural electrodes, respectively.^{32,36} Thus, each region of interest was represented as a volume in source space characterized by vertices with Euclidian distance < 5 or 10 mm (depending on the iEEG channel type) from each iEEG contact's centre. To reconstruct each VS's time series, we then computed the mean source activation of each VS (i.e. mean across volume points) for HD-EEG and MEG data, separately.^{30,32} Finally, these VSs' time series were used as inputs in FC analysis. For clarity, we will refer to those

VSs time series obtained from HD-EEG and MEG as HD-EEG-VSs and MEG-VSs, respectively [Fig. 1A(ii)].

Functional connectivity analysis

We filtered the iEEG, HD-EEG-VSs and MEG-VSs data between 1 and 50 Hz. We limited our analysis between 1 and 50 Hz to avoid spurious FC estimates due to ambient and/or biological artefacts in frequencies > 50 Hz, which are frequent in scalp EEG and MEG recordings from children,^{37,38} and to render our findings comparable with previous studies in the field.^{22,25,26,39–42} We identified data segments of 3-s duration characterized by specific activity patterns, i.e. epochs with and without (or minimal) IEDs [Fig. 1A(iii)] on each modality. Such selection allowed conducting two parallel analyses on different types of interictal activity, exploring how connectivity networks change in the presence or absence of frank interictal activity. Thus, for each signal (i.e. iEEG, HD-EEG-VSs and MEG-VSs), we analysed a total of 4 min of data (80 epochs of 3 s each) for each type of activity (with or without IEDs). We estimated undirected functional connections between regions with: (i) amplitude envelope correlation (AEC)^{43,44} and phase locking value (PLV)⁴⁵ [Fig. 1B(i)]. For minimizing the effect of source leakage,⁴⁶ we orthogonalized AEC before computing the correlation between each epoch's envelope. We computed AEC and PLV for different physiologically relevant frequency bands: delta (1–4 Hz), theta (4–8 Hz), alpha (8–12 Hz), beta (12–30 Hz), gamma (30–50 Hz) and broadband (1–50 Hz). Hence, we obtained two FC matrices for each epoch, characterized by $n \times n$ contacts that describe the pairwise connectivity between n number of nodes of the network corresponding to iEEG contacts or VSs [Fig. 1B(i)]. Finally, AEC and PLV matrices were averaged across epochs for data with and without IEDs.

To evaluate the consistency of FC over time, we performed a multiple comparison of AEC and PLV measures extracted from four randomly selected segments of iEEG, HD-EEG-VSs and MEG-VSs data (1-min duration each) using the Kruskal–Wallis test. For each signal, we found no significant differences among segments ($P > 0.05$) for any measure in data both with and without IEDs (Fig. 1C). Thus, we further analysed data of 1-min duration for each type of activity allowing direct comparison of our findings with previous studies showing that segments of this duration are sufficient to capture robust FC information.^{39,47}

Graph centrality analysis

The averaged AEC and PLV matrices represent each patient's brain activity as a graph consisting of a set of nodes equal to the number of iEEG contacts (or VSs) and edges equal to the inverted FC values.^{26,41} We used the minimum spanning tree (MST) to generate undirected subgraphs, characterized by n number of nodes with $(n - 1)$ inverted FC values.^{14,48} Such an approach maximizes the synchronizations among regions (i.e. minimizes the total edge connections) without forming loops between the connected nodes.^{14,41,48} For each patient, we estimated the MST from each AEC and PLV matrix, separately for data with and without IEDs of iEEG, HD-EEG-VSs and MEG-VSs signals [Fig. 1B(ii)]. We estimated the importance of each node (iEEG contact or VS) within the network by estimating graph centrality measures⁴⁹: (i) betweenness centrality: number of times a node act as a 'bridge' along the shortest path between two other nodes, defined as the fraction of all shortest paths passing through that node; (ii) closeness centrality: average length of the shortest path between the node and all graph

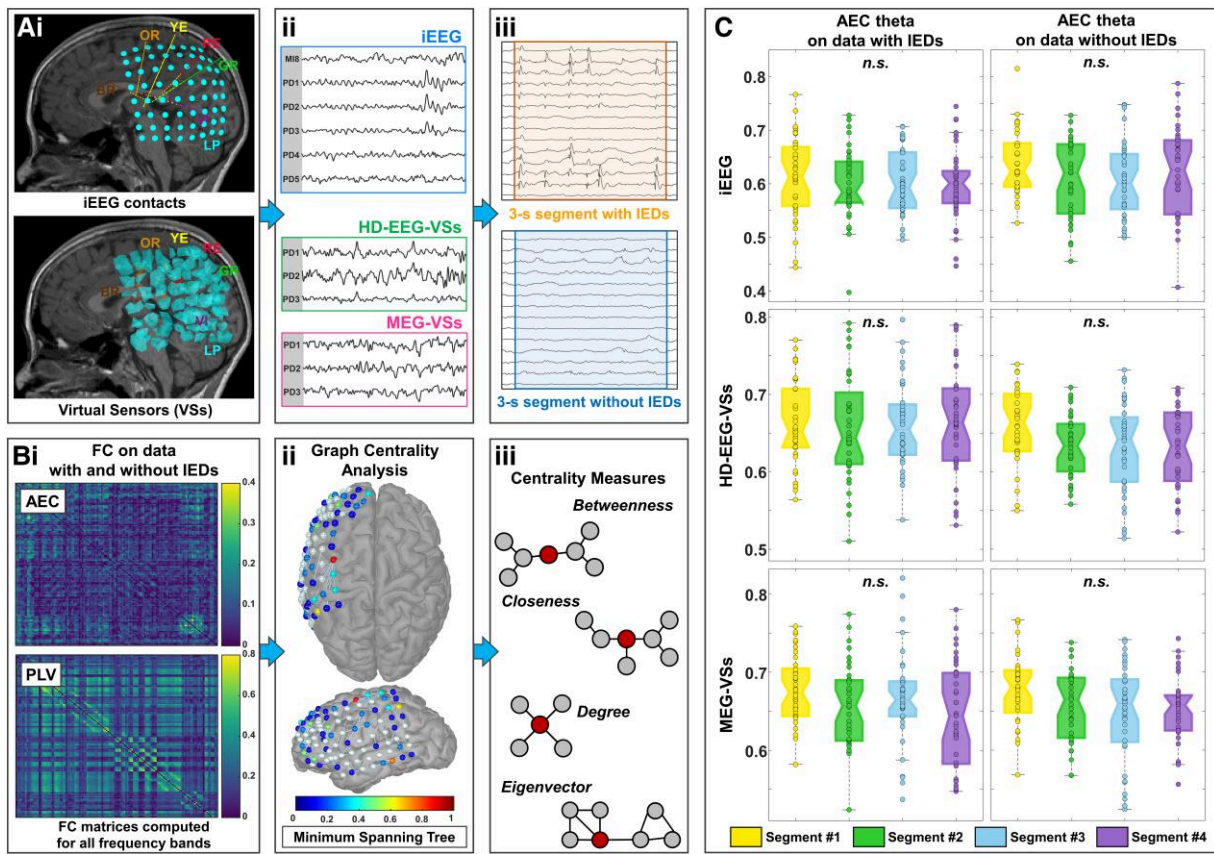


Figure 1 Overview of the data analysis pipeline. [A(i)] VSs reconstructed at brain locations that matched the iEEG implantation. (ii) For each VS, computation of its mean source activation across time acquired from data recorded by the HD-EEG and MEG sensors to reconstruct VS time series for HD-EEG (HD-EEG-VSs) and MEG (MEG-VSs), respectively. iEEG and VS time series filtered between 1 and 50 Hz. (iii) Selection of 4-min (80 epochs of 3-s duration each) data with and without IEDs on each signal (i.e. iEEG, HD-EEG-VSs and MEG-VSs). [B(i)] Computation of undirected FC between brain regions with amplitude envelope correlation (AEC) and phase locking value (PLV), for each frequency band, type of activity (data with and without IEDs) and signal (i.e. iEEG, HD-EEG-VSs and MEG-VSs). In each FC matrix, rows and columns represent the sensors (iEEG or VSs) and each pixel represents the pairwise connectivity of two selected sensors. (ii) Estimation of brain networks (as undirected subgraphs) from each FC matrix using the minimum spanning tree (MST) that maximizes the synchronizations between nodes (i.e. minimizes the total edge connections). Each node (iEEG contact or VS) of the brain network is colour-coded based on its FC value: connectivity range is from lower (0) to higher (1) values. (iii) Estimation of each node's importance within the network via four centrality measures of the MST: betweenness, closeness, degree and eigenvector. (C) Comparison of AEC measure across four segments (1-min duration each) on data with and without IEDs extracted from each signal (i.e. iEEG, HD-EEG-VSs and MEG-VSs). No significant differences were found among segments; n.s. = non-significant P-value ($P > 0.05$; Kruskal–Wallis test). In the box plots, the horizontal lines indicate the median value, lower and upper edges represent the 25th and 75th percentiles, whiskers extend to the minimum and maximum values (excluding outliers) and points outside the whiskers represent the outliers (i.e. values that are at least 1.5 times the interquartile range below the 25th percentile or above the 75th percentile).

nodes; (iii) degree: number of edges connected to a node; and (iv) eigenvector centrality: measure of the influence of the node, based on the quantity and quality of its connections [Fig. 1B(iii)].

Each FC measure (i.e. AEC, PLV and their relative centrality metrics) was normalized by its maximum value per patient.

Definition of resected areas

To identify which contacts were resected, we manually drew on consecutive slices the boundaries of the resected area by co-registering preoperative and postoperative MRIs and then computed the geometric (Euclidean) distance between each iEEG contact's centre (or VS) and the closest resection's margin. We then classified each contact (or VSs) as 'resected' or 'non-resected' if having a distance from resection below or above 10 mm, respectively.^{32,44} Geometric distance between brain network elements is a

parameter for modelling information transfer among regions^{50,51} and is related to FC measures.^{52,53} In epilepsy ESI/MSI studies, Euclidean distance from resection in patients with good versus poor outcome is regarded as a quantification measure of epileptogenicity.^{32,54,55} The assumption behind this notion is that a shorter distance to resection in patients with good outcomes (proof of successful EZ deactivation)—but not in poor-outcome patients—is an indicator of precise localization of the EZ.

Prediction of the EZ and surgical outcome

We defined the EZ as 'the area of cortex that is necessary and sufficient for initiating seizures and whose removal (or disconnection) is necessary for complete abolition of seizures'.⁵⁶ There is currently no direct preoperative measurement of the EZ; its delineation is a purely conceptual exercise incorporating data derived from

multiple tests and various components of presurgical evaluation.⁵⁷ Yet, rigorously quantified information about resection combined with surgical outcome data can serve as a proxy of the EZ.²⁰ Here, we presumed that in good-outcome patients, vital parts of the EZ were contained in the resection. In contrast, in poor-outcome patients, resection did not include critical EZ regions. Based on this presumption, we explored whether highly connected hubs can delineate the EZ and predict outcome.

To explore whether resection of highly connected hubs can delineate the EZ, we examined whether these hubs were located inside (or outside) the EZ in good-outcome patients. For each FC measure, we defined as true positive (TP) a resected node above threshold; as true negative (TN) a non-resected node below threshold; as false positive (FP) a non-resected node above threshold; and as false negative (FN) a resected node below threshold. The selected threshold ranged from 0% to 100% (5% step). We then calculated the positive (PPV = TP / [TP + FP]) and negative predictive values (NPV = TN / [TN + FN]), which were used to define prediction performance (PPV + NPV - 1) and accuracy ((TP + TN) / [TP + TN + FP + FN]). The optimal threshold to predict whether a node was inside (or outside) resection was the one with the highest performance.

To assess the association between highly connected hubs removal and outcome, we defined a threshold that varied from 0% to 100% (5% step) to classify each node with its own FC value in good- and poor-outcome patients. Considering nodes with FC above threshold, we tested whether their classification, as resected or non-resected, was confirmed by seizure-free state or not. We regarded as TP a resected node following by good outcome; as TN a non-resected node following by poor outcome; as FP a resected node following by poor outcome; and as FN a non-resected node following by good outcome. After estimating the PPV and NPV, we computed the prediction performance and accuracy. The best threshold that defined which nodes should be removed to predict outcome was the one with the highest performance.

Equivalent current dipoles

We marked IEDs on iEEG, HD-EEG and MEG independently, by selecting the peak of spike deflection.⁵⁴ IEDs of portions contaminated by biological artefacts were excluded from this analysis for all modalities. Source analysis was performed with an unconstrained equivalent current dipole (ECD) scanning method at the peak of each IED for all modalities.³⁰ Only ECDs with goodness-of-fit $\geq 60\%$ were considered.^{54,58}

For each ECD, we estimated its Euclidian distance from resection, and defined it as 'resected' if having a distance from resection ≤ 10 mm or 'non-resected' otherwise. Then, we tested the association between the ECDs' surgical removal and outcome. Based on TP, TN, FP and FN estimates, we computed the PPV and NPV that were then used to estimate the ECDs' prediction performance and accuracy.

Statistical analysis

To quantify the relationship between FC measures with the EZ, we performed a Wilcoxon signed-rank test comparing values between sensors inside versus outside resection, respectively, for good- and poor-outcome patients. The false discovery rate method was used to correct significance for multiple comparisons.⁵⁹ We tested both whether highly connected hubs were inside (or outside) resection and the association between their removal and patients' outcome using Fisher's exact test. Moreover,

Spearman's rank correlation was used to compare each measure estimated non-invasively with the same one estimated invasively, separate for resected and non-resected areas. Correlation coefficients between 0.4 and 0.7 were regarded as moderate, ≥ 0.7 as strong and ≥ 0.9 as very strong.⁶⁰ We also compared the averages of each FC measure inside resection with age at surgery (Spearman's rank correlation) and gender (Kruskal–Wallis test). Statistical analysis was performed in MATLAB®; we considered a statistical significance for $P < 0.05$.

Data availability

Data supporting the results of this study are available from the corresponding author upon request.

Results

Patient cohort

Thirty-seven patients (17 female, age at surgery: 2–23 years, mean: 13.7 years, median: 13.3 years) met our criteria. Median age at epilepsy onset was 4 years (range: 0–15) and median epilepsy duration prior to surgery was 9 years (range: 1–21). All patients had frequent disabling seizures before surgery. Patient demographics are summarized in Table 1. Eleven patients had normal MRI or subtle lesion of doubtful clinical significance. Seizures were recorded from the dominant and non-dominant hemispheres in 21 (56.76%) and 16 (43.24%) patients, respectively.

iEEG data were recorded through the implantation of subdural (13 patients), depth (10 patients) or both types of electrodes (14 patients). We analysed an average of 22.09 min (range: 4.82–67.50) of iEEG data from a mean number of 120 (range: 64–236) channels and 12.14 min (range: 11.9–12.6) of HD-EEG and MEG data. We excluded a mean of four channels for iEEG and 17 channels for HD-EEG and MEG owing to artefacts. We performed ECDs fitting on an average number of 239.4 (range: 56–627), 49.2 (range: 6–226) and 62.2 (range: 6–436) IEDs for the iEEG, HD-EEG and MEG data, respectively. The mean resected volume was 24.07 ± 20.12 cm³ (range: 1.81–74.89). Twenty-two patients (59.5%) had good outcome [median: 5 years (range: 2–9) post-surgery]. We did not find differences between good- and poor-outcome patients in terms of age at epilepsy onset (Wilcoxon rank-sum test, $P = 0.82$), epilepsy duration prior to surgery (Wilcoxon rank-sum test, $P = 0.85$), pathology (Pearson chi-squared test, $P = 0.44$), gender (Fisher's exact test, $P = 0.19$) or resection location (Fisher's exact test, $P = 0.71$).

Functional connectivity on iEEG

We observed increased FC inside (compared to outside) resection in good-outcome patients for: (i) AEC in theta ($P = 0.006$), alpha ($P = 0.010$), beta ($P = 0.010$), gamma ($P < 0.001$) and broad ($P = 0.016$) bands on data with IEDs (Fig. 2A); (ii) AEC in theta ($P = 0.014$) and gamma ($P = 0.003$) bands on data without IEDs (Fig. 2A); and (iii) PLV in alpha ($P = 0.005$) on data with IEDs. Few differences were found in poor-outcome patients [i.e. AEC alpha ($P = 0.007$), beta ($P = 0.004$) and gamma ($P = 0.003$)] only on data with IEDs.

We observed increased centrality inside resection in good-outcome patients for all metrics computed from AEC or PLV on data with and without IEDs across different bands (Table 2). Few differences were found in poor-outcome patients (Table 2). All P -values were corrected for multiple comparisons using FDR.

Table 1 Patient demographics

ID/Sex	Age, ^a years	Epilepsy onset, years	iEEG (n)	Side	MRI findings	Pathology	Engel	ILAE (f/u, years)	Resection volume, cm ³
1/M	11	4	SE (80)	R	Normal	NL	IA	I (5)	13.09
2/M	11	2	SE, DE (88 + 10)	L	Normal	DEV	IA	I (4)	8.24
3/F	7	3	DE (90)	L	FCD (T and Ins)	DEV	IB	III (8)	13.7
4/F	11	8	SE, DE (144 + 10)	R	Normal	DEV	IA	I (6)	55.92
5/F	10	0.3	DE (140)	L	Hippocampal sclerosis	DEV	IVB	V (6)	8.48
6/F	14	10	SE (72)	L	Normal	NL	IA	I (5)	18.66
7/M	18	9	SE, DE (72 + 20)	L	Tumour (T)	ACQ	IC	I (6)	38.54
8/M	2	0.3	SE (112)	R	TSC (multifocal)	DEV	IA	I (7)	53.79
9/F	9	4	SE, DE (80 + 20)	R	FCD (P)	DEV	IIIA	IV (9)	23.71
10/M	19	8	SE (64)	L	FCD (mesial T)	DEV	IA	I (4)	32.39
11/F	18	15	DE (88)	L	Normal	NL	IA	I (7)	26.79
12/M	16	4	DE (88)	L	Normal	NL	IA	I (5)	10.9
13/M	20	4	DE (88)	L	Mild gliosis	Unknown	IIIA	IV (5)	5.81
14/M	18	1.5	DE (128)	R	Known resection cavity P-O	DEV	IIIA	IV (4)	15.8
15/F	10	1	SE, DE (112 + 10)	R	Low-grade neoplasm (Fr)	ACQ	IB	II (4)	25.21
16/F	19	4	SE, DE (144 + 10)	L	FCD (Fr)	DEV	IA	I (3)	7.38
17/F	15	6	SE (72)	L	FCD (mesial P)	DEV	IIIA	IV (6)	8.18
18/M	13	8	SE, DE (72 + 30)	L	Encephalomalacia (P, superior T)	ACQ	IC	I (3)	13.36
19/M	13	7	SE, DE (112 + 10)	L	FCD (T)	DEV	IIIA	V (6)	69.85
20/M	13	0	SE (136)	L	Infarct (MCA territory)	ACQ	IC	I (5)	47.26
21/M	23	5	SE, DE (64 + 30)	L	FCD	DEV	IA	I (3)	21.86
22/F	12	1	DE (70)	L	Normal	DEV	IA	I (4)	29.58
23/M	13	1.5	SE (92)	L	FCD (mesial T)	DEV	IA	I (9)	45.5
24/M	18	5	DE (212)	L	FCD	DEV	IIIA	V (6)	4.64
25/F	23	14	SE (120)	R	Bilateral	ACQ	IIB	III (5)	24.04
26/M	10	7	SE, DE (64 + 60)	L	Polymicrogyria (Fr, P)	DEV	IIIA	IV (7)	59.97
27/F	10	8	SE (96)	L	FCD (F)	DEV	IIIA	V (5)	1.81
28/F	7	4	SE, DE (72 + 40)	R	FCD (Fr operculum)	DEV	IC	I (8)	8.91
29/M	4	2	SE, DE (128 + 10)	R	R frontal pole, superior Fr gyrus	DEV	IIIA	IV (4)	74.89
30/F	16	3	DE (212)	L	Normal	NL	IIIA	IV (5)	4.07
31/M	23	2	DE (162)	L	Normal	DEV	IA	I (5)	52.07
32/F	8	6	DE (164)	L	FCD (posterior Fr)	DEV	IA	I (4)	12.42
33/M	15	6	DE (102)	R	Normal	DEV	IA	I (2)	7.64
34/F	18	3	SE, DE (72 + 40)	L	FCD (Fr)	DEV	IA	I (2)	5.42
35/M	15	6	DE (236)	L	Normal	NL	IC	I (4)	19.06
36/M	13	0	SE, DE (72 + 24)	L	Inferior Fr sulcus, pars Tr	DEV	IC	I (5)	16.79
37/F	15	3.5	DE (166)	L	Hippocampal asymmetry	ACQ	IIIA	IV (4)	4.93

ACQ = acquired (i.e. stroke, neoplasm and traumatic brain injury); DE = depth electrodes (stereo-EEG); DEV = malformation of cortical development (i.e. focal cortical dysplasia, polymicrogyria, tuberous sclerosis complex, dysembryoplastic neuroepithelial tumour and glioma); F = female; FCD = focal cortical dysplasia; f/u = follow-up; Fr = frontal; IE = inter-hemispheric; Ins = insula; L = left; M = male; MCA = middle cerebral artery; NL = non-lesional; O = occipital; P = parietal; R = right; Res = resection; SE = subdural electrodes (electrocorticography); T = temporal; Tr = triangularis; TSC = tuberous sclerosis complex.

^aAge = age at epilepsy surgery.

Functional connectivity on virtual sensors

For the HD-EEG-VSs, we observed higher FC inside resection in good-outcome patients for: (i) AEC in alpha ($P=0.001$), beta ($P=0.001$), gamma ($P=0.008$) and broad ($P=0.002$) bands on data without IEDs; and (ii) PLV in delta ($P=0.042$), theta ($P=0.033$) and alpha ($P=0.039$) bands on data without IEDs. We did not observe differences for poor-outcome patients. For the MEG-VSs, good-outcome patients showed increased FC inside resection for: (i) AEC in beta band ($P=0.006$) on data with IEDs; (ii) AEC in beta ($P=0.013$) and broad ($P=0.005$) bands on data without IEDs; (iii) PLV in all bands (delta: $P=0.017$; theta: $P=0.011$; alpha: $P=0.012$; beta: $P=0.007$; gamma: $P=0.002$; broadband: $P=0.009$) on data with IEDs; and (iv) PLV in all bands (delta: $P=0.050$; theta: $P=0.022$; alpha: $P=0.019$; beta: $P=0.009$; gamma: $P=0.002$; broadband: $P=0.012$) on data without IEDs. We did not observe differences for poor-outcome patients. P -values were corrected for multiple comparisons using FDR.

Good-outcome patients showed increased centrality for the HD-EEG-VSs inside resection for: (i) PLV closeness and eigenvector on data with and without IEDs; and (ii) AEC degree on data without IEDs (Table 2). We did not observe differences for poor-outcome patients, except for PLV closeness on data without IEDs (Table 2). MEG-VSs showed centrality differences among resected versus non-resected areas in good-outcome patients for: (i) PLV closeness on data with IEDs; and (ii) PLV betweenness and closeness on data without IEDs (Table 2). We did not observe differences for poor-outcome patients.

Comparison with benchmark

Several FC metrics computed non-invasively provided similar results as those computed invasively, with significant increases ($P < 0.05$) of FC located inside resection (compared to outside) for good-outcome patients. Thus, some measures computed from iEEG shared these differences only with one of the two VSs modalities,

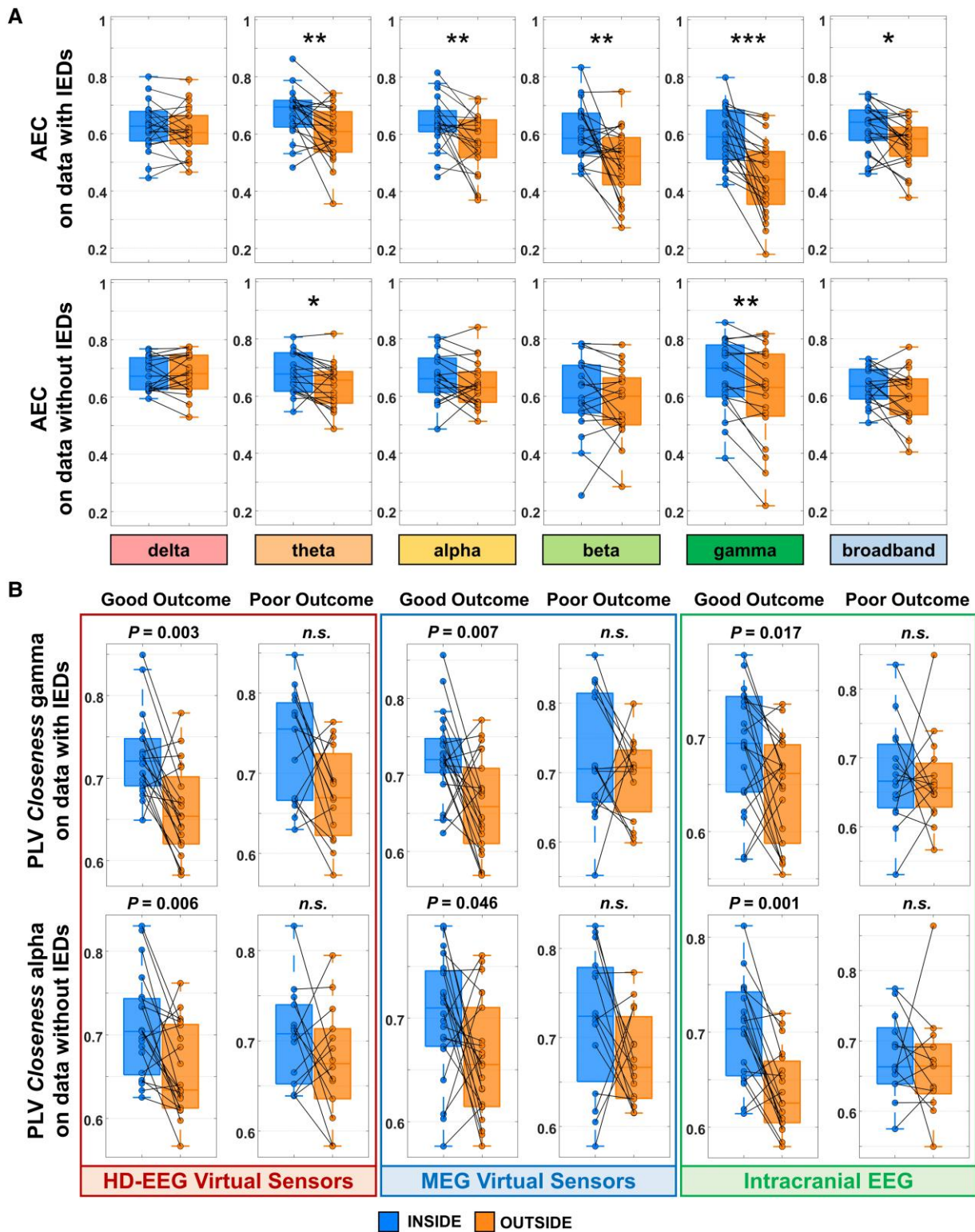


Figure 2 FC findings of iEEG and VS analyses. (A) AEC computed on iEEG data with and without IEDs for good-outcome patients inside versus outside resection for the delta, theta, alpha, beta, gamma and broad frequency bands. Significant differences are indicated by asterisks: * $P < 0.05$, ** $P < 0.01$, *** $P < 0.001$ (P -values corrected for multiple comparisons using the FDR method). (B) PLV closeness on data with (for the gamma band) and without (for the alpha band) IEDs for patients with good and poor surgical outcome inside versus outside resection. PLV values are displayed for HD-EEG-VSs, MEG-VSs and iEEG data. FC values inside resection are displayed in the left box plot of each panel; FC values outside resection are displayed in the right box plot of each panel; P -values (Wilcoxon signed-rank test) are corrected for multiple comparisons using the FDR method; *n.s.* = not significant P -value. In the box plots, the horizontal line indicates the median value, lower and upper edges represent the 25th and 75th percentiles, whiskers extend to the minimum and maximum values (excluding outliers) and points outside the whiskers represent the outliers (i.e. values that are at least 1.5 times the interquartile range below the 25th percentile or above the 75th percentile).

Table 2 FC measures from invasive and non-invasive (VSs) data

iEEG								
	Betweenness		Closeness		Degree		Eigenvector	
	Good	Poor	Good	Poor	Good	Poor	Good	Poor
AEC								
Delta								
Theta	0.005 (0.001)		0.004 (0.002)		0.007 (0.004)		(0.002)	0.002
Alpha			0.019					0.008
Beta		0.008		0.002		0.012		
Gamma	0.001	0.005	0.003 (0.005)	0.004	***	0.003	0.016	
Broadband								
PLV								
Delta	0.031 (0.011)							
Theta	0.039 (0.010)				0.007			
Alpha	0.002 (0.003)		0.003 (0.001)					
Beta	0.016 (0.040)		0.005					
Gamma	0.050 (0.049)		0.017					
Broadband	0.005 (0.033)							
ESI								
	Betweenness		Closeness		Degree		Eigenvector	
	Good	Poor	Good	Poor	Good	Poor	Good	Poor
AEC								
Delta								
Theta								
Alpha					(0.002)			
Beta								
Gamma								
Broadband								
PLV								
Delta			0.014 (0.006)					
Theta			0.033 (0.050)	(0.004)				
Alpha			0.014 (0.006)					
Beta			0.006 (***)				(0.006)	
Gamma			0.003 (***)				0.007 (0.002)	
Broadband			0.048 (0.002)				(0.012)	
MSI								
	Betweenness		Closeness		Degree		Eigenvector	
	Good	Poor	Good	Poor	Good	Poor	Good	Poor
AEC								
Delta								
Theta								
Alpha								
Beta								
Gamma								
Broadband								
PLV								
Delta								
Theta	(0.022)		(0.002)					
Alpha	(0.050)		(0.046)					
Beta	(0.013)		(0.004)					
Gamma			0.007 (0.004)					
Broadband	(0.031)		(0.013)					

Values are presented as data with IEDs (data without IEDs). Empty cells represent the non-statistical significance of the measure of interest for that specific surgical outcome. Statistically significant P-values (Wilcoxon signed-rank test) after FDR correction are displayed; ***P < 0.001.

and only in few cases with both (Table 2). Examples of congruent results among all modalities are shown in Fig. 2B. To highlight the relationship of highly connected hubs with the EZ, we mapped the PLV closeness alpha for two representative patients: one with good and one with poor outcome (Fig. 3). For the good-outcome patient, we observed high FC mostly within the EZ and lower FC in distant regions. Notably, non-invasive FC measures were concordant with invasive ones. Contrarily, we observed high FC in several non-resected regions for the poor-outcome patient.

At the population level, we found moderate correlations for HD-EEG-VSs and MEG-VSs versus iEEG for several AEC and PLV centrality measures for resected areas, as well as for non-resected areas (Supplementary Table 1). FC measures did not correlate with either age at surgery or gender except a few of them. We found a weak correlation between AEC eigenvector (broadband) on data with IEDs and age ($\rho < 0.4$, $P < 0.05$). This measure was also correlated with gender ($P = 0.044$). AEC degree (delta) on data without IEDs was correlated with age ($\rho < 0.4$, $P < 0.05$) and AEC degree (theta) on data with IEDs was correlated with gender ($P = 0.010$). In Fig. 4, we report correlation results ($\rho \geq 0.4$, $P < 0.05$) at the patient level of FC measures between iEEG and VSs analyses, as well as between HD-EEG-VSs and MEG-VSs for resected (Fig. 4A) and non-resected (Fig. 4B) areas. Comparing iEEG with HD-EEG-VSs, we found that 92%, 16% and 3% of patients obtained moderate, strong and very strong correlations, respectively, for resected areas, whereas for non-resected areas, we found 86% and 19% of patients that showed moderate and strong correlations, respectively (Supplementary Table 1). Comparing iEEG with MEG-VSs, we observed that 89% and 13% of patients showed moderate and strong correlations, respectively, for resected areas, as well as 89% and 22% of patients who obtained these findings for non-resected areas (Supplementary Table 1).

Prediction of EZ and outcome

For the iEEG FC measures in good-outcome patients, we found that resection of highly connected hubs predicted the EZ for the: (i) AEC (gamma) and PLV betweenness (theta and beta) with PPVs = 73% and NPVs = 61% on data with IEDs; and (ii) AEC betweenness, closeness and eigenvector (theta) with PPVs $\geq 74\%$ and NPVs $\geq 60\%$, on data without IEDs. Furthermore, we found that other FC measures were predictive of the EZ (Supplementary Table 2). For the HD-EEG-VSs FC measures in good-outcome patients, resection of highly connected hubs predicted the EZ for the: (i) AEC betweenness and closeness (broadband) and PLV eigenvector (theta and gamma) with PPVs $\geq 75\%$ and NPVs $\geq 60\%$ on data with IEDs; and (ii) AEC betweenness (broadband) and PLV eigenvector (gamma) with PPVs $\geq 75\%$ and NPVs = 61% on data without IEDs. Other FC metrics were predictive of the EZ for the HD-EEG-VSs (Supplementary Table 3). For the MEG-VSs FC measures in good-outcome patients, resection of highly connected hubs predicted the EZ for the: (i) PLV (alpha and beta) with PPVs = 73% and NPVs = 61% on data with IEDs; and PLV (theta and gamma) with PPVs $\geq 73\%$ and NPVs = 61% on data without IEDs. Other predictive metrics of the EZ are presented in Supplementary Table 4. To validate our results, we performed leave-one-out cross-validation using all patients but one as training set, repeatedly for 37 (total number of patients) times, separately for each analysis. These results are summarized in Supplementary Tables 2–4.

For iEEG, hubs resection predicted outcome for PLV closeness (gamma and theta) on data with and without IEDs (Fig. 5A). For HD-EEG-VSs, hubs resection predicted outcome for PLV betweenness (gamma and alpha) on data with and without IEDs (Fig. 5A).

For MEG-VSs, hubs resection predicted outcome for PLV betweenness (gamma) on data with and without IEDs (Fig. 5A). For each measure, the leave-one-out cross-validation results are summarized in Table 3, together with other predictive measures in different bands. FC measures that predicted both the EZ in good-outcome patients as well as the surgical outcome are reported in Table 3.

To assess if the predictive network hubs were located within the EZ, we investigated whether their distance from resection was lower in good- versus poor-outcome patients (Wilcoxon rank-sum test). For each patient, we therefore considered hubs of those FC metrics (Table 3) that had values above (or equal) to their connectivity thresholds and extracted their distance from resection for iEEG, HD-EEG-VSs and MEG-VSs, separately. For those patients who had more than one hub with FC higher than their threshold, we computed their mean distance from resection. From the iEEG prediction analysis, we found that hubs of PLV (delta, alpha, gamma and broadband) on data with IEDs had lower distance from resection in good- versus poor-outcome patients ($P = 0.025$, $P = 0.046$, $P = 0.014$ and $P = 0.034$). From the HD-EEG-VSs prediction analysis, we found hubs with lower distance from resection in good- versus poor-outcome patients for: (i) PLV (theta) on data with IEDs ($P = 0.019$); (ii) AEC (alpha; $P = 0.010$), PLV (delta, beta and broadband; $P = 0.003$, $P = 0.015$ and $P = 0.013$) on data without IEDs; (iii) PLV betweenness (theta, beta, gamma and broadband; $P = 0.001$, $P = 0.022$, $P = 0.001$ and $P = 0.044$) and eigenvector (gamma; $P = 0.047$) on data with IEDs; and (iv) PLV betweenness (alpha and gamma; $P = 0.045$ and $P = 0.011$) and eigenvector (gamma; $P = 0.015$) on data without IEDs. From the MEG-VSs prediction analysis, we observed that hubs of PLV betweenness and closeness (gamma; $P = 0.046$ and $P = 0.037$) on data with IEDs and PLV eigenvector (delta; $P = 0.025$) on data without IEDs showed lower distances from resection in good- versus poor-outcome patients.

Outcome prediction through FC metrics (from iEEG and VSs) obtained better results compared to ECDs (Fig. 5B), which did not show significance in any modality. Although ECDs did not predict outcome, they identified dipoles within resection in good-outcome patients (PPV = 100%) both for HD-EEG and MEG.

Discussion

We here propose a novel non-invasive method that maps epileptogenic networks and identifies pathological hubs in the brain of patients with DRE through the ‘implantation’ of VSs based on ESI/MSI. By applying this method on interictal MEG and HD-EEG data, we non-invasively reconstruct brain signals with similar FC features with those obtained invasively through iEEG and predict non-invasively the EZ and the patient’s surgical outcome—even in the absence of frank epileptiform activity—better than conventional source localization. This notion derives from our main findings: (i) higher FC for interictal iEEG data (with and without IEDs) recorded from contacts inside resection for patients with good outcome; (ii) higher FC inside resection for interictal MEG and HD-EEG data (with and without IEDs) estimated via VSs in good-outcome patients; (iii) highly connected hubs predicted the EZ in good-outcome patients; (iv) moderate and strong correlations between invasive and non-invasive FC at population- and patient-level; (v) resection of highly connected hubs, identified by both invasive and non-invasive methods, were associated with good outcome for data with and without IEDs; (vi) hubs (predictive of outcome) computed from both invasive and non-invasive data are closer to resection in good- than poor-outcome patients; (vii) hubs overlapped with resection in $\geq 60\%$ of good-outcome patients; and (viii) conventional

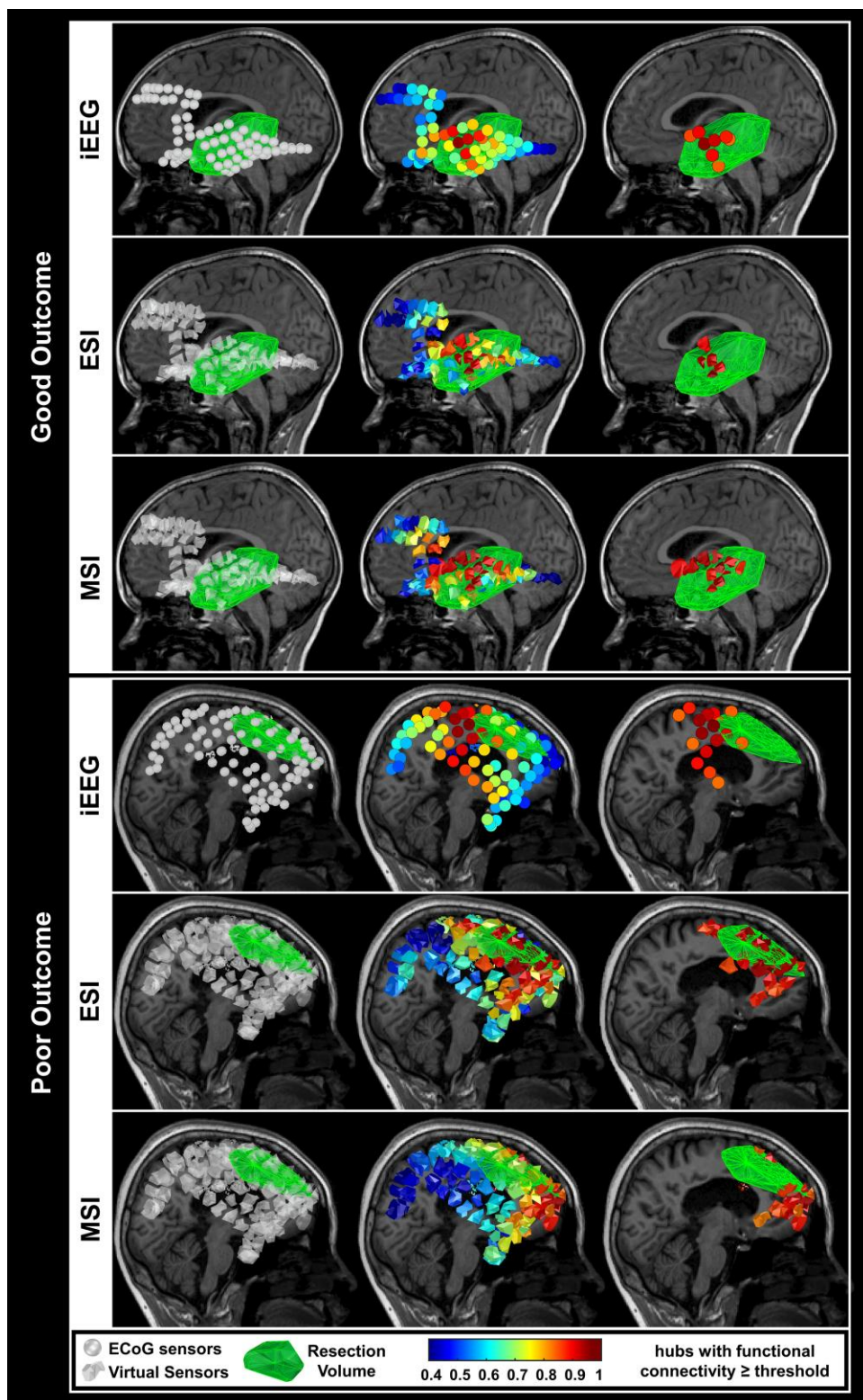


Figure 3 FC results for a patient with good and poor surgical outcome. Left: Relative location of electrodes for iEEG and VSs for HD-EEG and MEG with respect to patients' preoperative MRI [Patient 23 (ILAE I) and Patient 25 (ILAE III)]. Resected zone is displayed as a volume. Middle: Heat maps of PLV closeness estimated on data without IEDs in the alpha frequency band. Connectivity range is from lower (0.4) to higher (1) values. Right: Representation of pathological hubs (i.e. nodes with FC higher than a threshold) for the good- and poor-outcome patients; for visualization purposes, FC values ≥ 0.85 are displayed. ECoG=electrocorticography; ESI=electric source imaging (through HD-EEG-VSs); MSI=magnetic source imaging (through MEG-VSs).

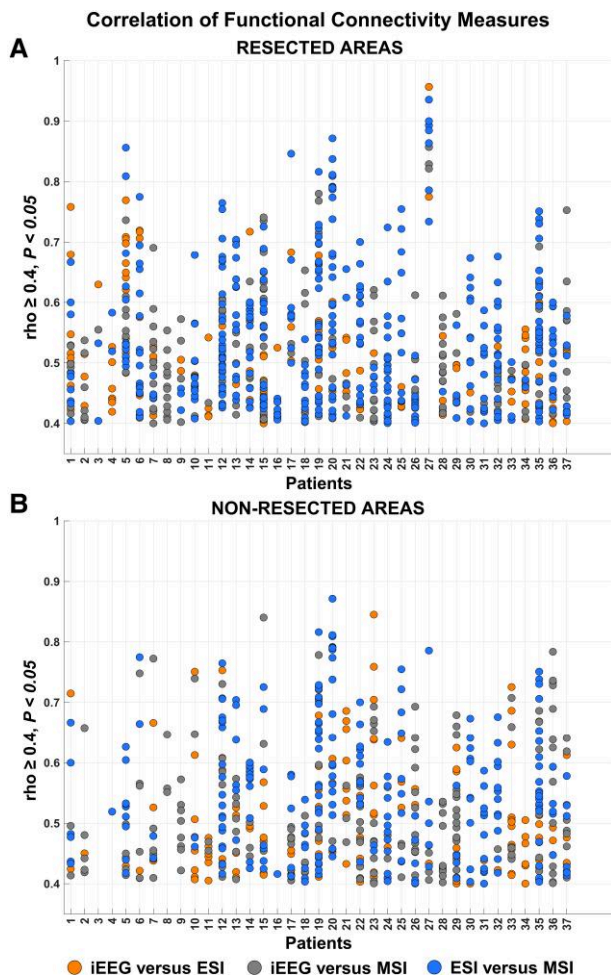


Figure 4 Correlation results of FC measures at the patient's level. For each patient, correlation coefficients (ρ) were obtained by comparing normalized FC measures of (i) iEEG with the same ones of electric source imaging (ESI; i.e. HD-EEG-VSs); (ii) iEEG with the same ones of MSI (i.e. MEG-VSs); and of (iii) ESI with the same ones estimated through MSI. Correlation coefficients ≥ 0.4 ($P < 0.05$) are displayed for both resected areas (top) and non-resected areas (bottom). Correlation coefficients between 0.4 and 0.7 are regarded as moderate, ≥ 0.7 as strong and ≥ 0.9 as very strong (Spearman's rank correlation).

ESI/MSI with ECDs did not predict outcome in contrast to FC measures.

Functional connectivity is higher inside the EZ for interictal iEEG data with and without IEDs

Several iEEG studies have shown that FC is a potentially useful biomarker for the EZ delineation.^{17,18,20} Yet, most of these studies analyse either ictal or pre-ictal data.^{42,61} More recent evidence suggests that interictal recordings are also informative for delineating the epileptogenic network.¹⁹ Nevertheless, the available findings are contradictory: most studies report increased FC in more epileptogenic areas compared to others,^{16–18,20,26,42,61} but others report the opposite effect.^{41,47,62} Moreover, only few iEEG studies relate FC with outcome.^{20,42} Thus, despite extensive literature in the field, network organization in epilepsy remains incompletely understood. Here, we fill this gap by correlating the removal of highly connected hubs with favourable outcomes. Our iEEG data indicate a

relationship between FC and the EZ. More importantly, they provide an added value for predicting the EZ. We observed increased FC inside resection for good-outcome patients but very few differences in poor-outcome patients. High FC was found in all frequency bands (except delta for AEC); yet the findings were more prominent in the theta and gamma bands for AEC and alpha band for PLV, in line with previous studies.^{16,17} We also observed increased centrality inside resection for all metrics on data with and without IEDs across different bands. In summary, FC measures, such as AEC and PLV, and their estimated graph-theory metrics, can predict the EZ even in the absence of IEDs.

Functional connectivity is higher inside the EZ for non-invasively estimated virtual sensor data

Several non-invasive studies have explored source-space FC as a biomarker of the EZ.^{25,39,47,63} Most of them explore brain regions that generate and spread seizures to the rest of the network revealing abnormal connectivity alterations that differ from those of healthy controls.^{47,63–65} It is still largely unknown how reliable these non-invasive FC findings are compared to the ones estimated via iEEG. So far, only one MEG study correlated FC measures derived from VSs with those obtained from iEEG,²⁶ showing how invasive time series can be non-invasively approximated with VSs. By comparing iEEG and MEG, Juárez-Martínez et al.²⁶ found correlations for spectral metrics and FC, and highly central nodes included in resected areas. Similarly, Cao et al.²⁷ reported that reconstructed virtual iEEG signals from ictal MEG have morphological and spatial characteristics comparable with ictal iEEG, and their FC estimates can help identify the EZ and predict its clinical localization.²⁷ Yet, MEG is blind to deep generators or those having radial orientation, such as activity at the gyral crowns or sulcal depths,⁶⁶ and thus it may provide an incomplete estimation of the epileptiform activity derived from these sources. Here, we correlate functional networks computed via VSs from both HD-EEG and MEG data with the ones estimated with iEEG. Using VSs, we observed the same connectivity trend as with iEEG, in which FC was increased inside resection in good- but not in poor-outcome patients. These source-level connectivity findings were consistent on data with and without IEDs. With HD-EEG-VSs, we obtained increased AEC and PLV within resection of good-outcome patients in all frequencies (except delta and theta for AEC and beta, gamma and broadband for PLV), while with MEG-VSs, for AEC in beta and broad bands and for PLV in all frequencies. These findings are in line with previous studies^{47,64} showing that increased connectivity (at the source level) predicts accurate localization of the EZ. Here, we report similar findings from both interictal MEG and HD-EEG showing their ability to provide complementary information to the iEEG. Overall, our findings indicate that highly connected brain regions, estimated non-invasively via VSs, can localize the EZ in the brain of children and young adults with DRE even in the absence of frank epileptiform activity on MEG or HD-EEG recordings.

Interictal functional connectivity predicts outcome outperforming conventional methods

To establish a relationship between FC and outcome, we investigated the role of network hubs in propagating the epileptogenic activity across regions by assessing if their resection leads to favourable outcome. Previous studies have shown that seizure-freedom is associated with resection of regions containing pathological hubs.^{25,39} Here, we report findings from interictal iEEG,

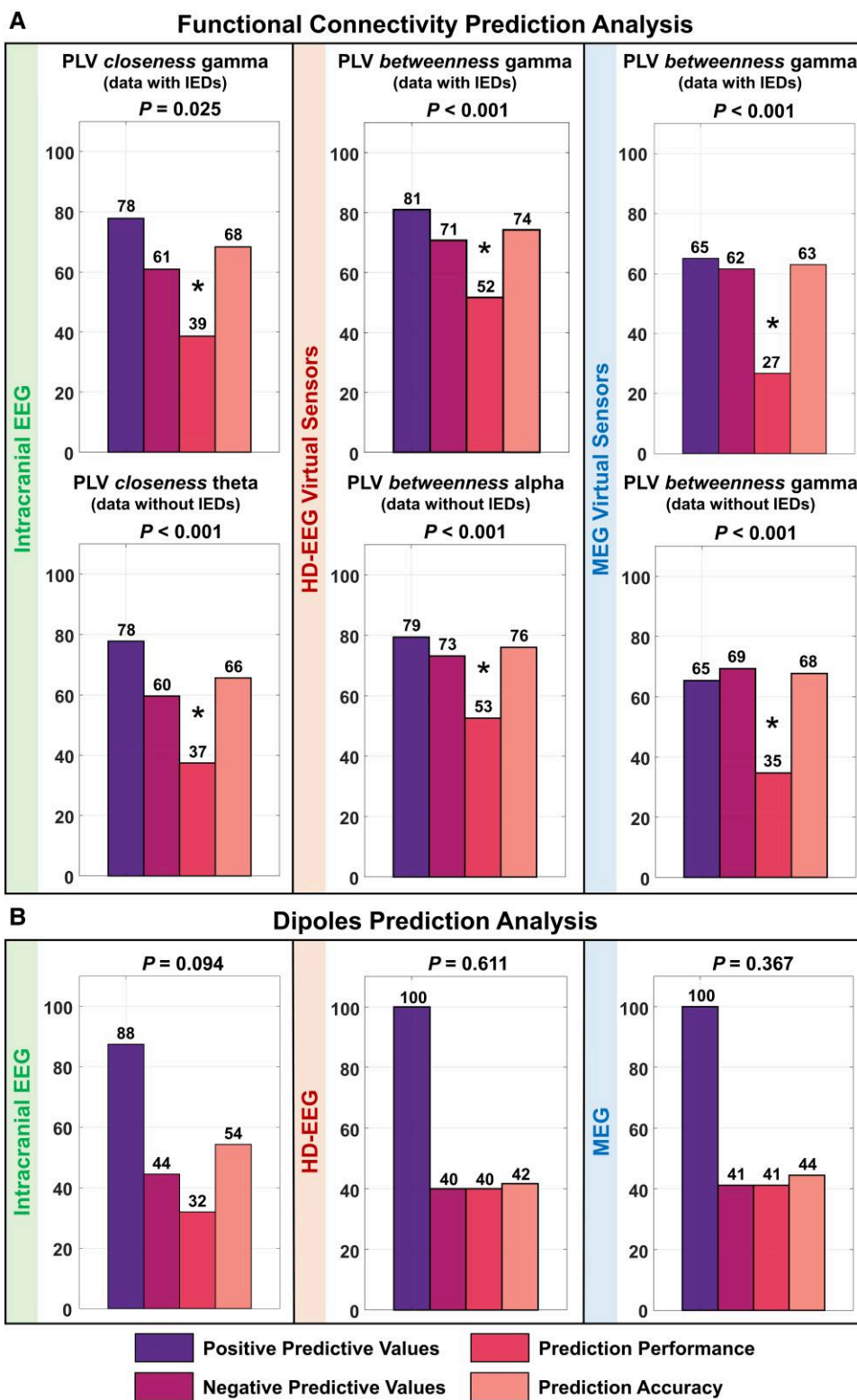


Figure 5 Surgical outcome prediction results. (A) Resection of network hubs (i.e. brain regions with high FC) was associated with good surgical outcome for the: (i) PLV closeness at gamma and theta bands on data with and without IEDs, respectively, for iEEG; (ii) PLV betweenness at gamma and alpha bands on data with and without IEDs, respectively, for HD-EEG-VSSs; and (iii) PLV betweenness at gamma band on data with and without IEDs for MEG-VSSs. P-values < 0.05 are displayed (Fisher's exact test). (B) Resection of dipoles computed at the peak of each IED was not predictive of surgical outcome for iEEG, HD-EEG and MEG (P > 0.05; Fisher's exact test).

Table 3 Prognostic value of FC: leave-one-out cross-validation

	Threshold (%)	Fisher's exact test	Performance	PPV	NPV	Accuracy
iEEG						
PLV broadband ^{a,b}	100	0.045	36 (33–40%)	78 (76–82%)	58 (56–61%)	68 (67–69%)
PLV delta ^{a,b}	100	0.045	36 (33–40%)	78 (76–82%)	58 (56–61%)	68 (67–69%)
PLV alpha ^a	95	0.017	21 (12–30%)	60 (57–65%)	61 (52–69%)	61 (55–66%)
PLV gamma ^a	95	***	31 (22–36%)	67 (60–74%)	64 (55–73%)	65 (59–69%)
PLV gamma ^c	95	***	32 (22–37%)	69 (63–76%)	63 (53–72%)	65 (58–70%)
PLV degree delta ^{a,b}	75	0.002	19 (13–26%)	59 (53–66%)	60 (52–67%)	60 (57–63%)
PLV degree theta ^a	75	***	22 (14–28%)	61 (56–68%)	61 (52–66%)	61 (57–63%)
PLV eigenvector theta ^a	50	0.024	18 (14–22%)	63 (58–68%)	55 (51–59%)	59 (56–61%)
PLV betweenness alpha ^{a,b}	85	0.012	25 (18–31%)	65 (60–69%)	60 (50–67%)	63 (60–65%)
PLV closeness alpha ^a	95	***	26 (22–31%)	67 (62–72%)	59 (53–66%)	64 (60–66%)
PLV closeness gamma ^a	100	0.025	39 (35–43%)	78 (76–82%)	61 (57–64%)	68 (67–70%)
PLV betweenness theta ^c	80	***	26 (22–36%)	68 (62–77%)	58 (50–74%)	62 (59–69%)
PLV closeness theta ^c	95	***	37 (30–45%)	78 (74–82%)	60 (51–71%)	66 (61–72%)
ESI						
AEC beta ^{a,b}	90	***	26 (19–30%)	57 (52–63%)	68 (61–74%)	63 (59–65%)
PLV theta ^{a,b}	95	0.003	25 (21–31%)	69 (67–75%)	56 (51–62%)	62 (60–64%)
AEC alpha ^{b,c}	100	0.041	37 (34–41%)	78 (76–82%)	59 (56–62%)	69 (68–71%)
PLV broadband ^{b,c}	100	0.041	37 (34–41%)	78 (76–82%)	59 (56–62%)	69 (68–71%)
PLV delta ^{b,c}	100	0.015	43 (41–49%)	82 (81–87%)	61 (59–65%)	71 (71–73%)
PLV beta ^{b,c}	100	0.041	37 (34–41%)	78 (76–82%)	59 (56–62%)	69 (68–71%)
AEC betweenness broadband ^{a,b}	95	0.012	42 (39–50%)	74 (71–81%)	68 (65–76%)	71 (70–75%)
AEC closeness broadband ^{a,b}	100	0.041	38 (33–43%)	71 (70–75%)	67 (61–71%)	69 (68–71%)
AEC betweenness beta ^{a,b}	55	0.007	25 (20–31%)	65 (62–73%)	59 (54–63%)	62 (60–65%)
AEC closeness beta ^{a,b}	85	0.035	19 (13–22%)	63 (60–68%)	56 (50–59%)	59 (57–61%)
AEC degree beta ^{a,b}	70	0.006	30 (22–34%)	63 (57–67%)	67 (59–71%)	65 (61–67%)
AEC closeness gamma ^{a,b}	70	***	25 (19–30%)	68 (65–73%)	57 (50–61%)	62 (59–64%)
PLV betweenness broadband ^a	95	0.009	41 (34–46%)	82 (79–87%)	59 (51–62%)	66 (62–68%)
PLV betweenness theta ^{a,b}	100	0.015	44 (42–50%)	81 (80–87%)	63 (61–67%)	71 (71–73%)
PLV eigenvector theta ^{a,b}	95	0.009	43 (38–47%)	78 (75–82%)	65 (60–69%)	72 (70–74%)
PLV betweenness beta ^{a,b}	95	0.038	32 (26–40%)	76 (74–80%)	56 (50–64%)	65 (63–70%)
PLV betweenness gamma ^{a,b}	95	***	52 (40–56%)	81 (79–85%)	71 (59–74%)	74 (68–76%)
PLV eigenvector gamma ^{a,b}	95	0.007	48 (46–52%)	79 (78–83%)	69 (67–73%)	74 (73–76%)
AEC betweenness broadband ^{b,c}	100	0.007	40 (38–45%)	76 (75–80%)	64 (61–69%)	71 (71–73%)
AEC closeness beta ^c	85	***	24 (18–27%)	65 (61–70%)	59 (53–63%)	61 (58–64%)
PLV betweenness broadband ^{b,c}	85	***	39 (34–48%)	78 (74–84%)	61 (54–74%)	67 (63–74%)
PLV closeness delta ^c	95	***	30 (26–33%)	67 (64–70%)	62 (58–67%)	64 (62–66%)
PLV betweenness alpha ^{b,c}	90	***	53 (46–58%)	79 (77–84%)	73 (67–79%)	76 (73–79%)
PLV eigenvector alpha ^{b,c}	65	0.019	24 (17–28%)	66 (63–70%)	58 (51–61%)	62 (59–64%)
PLV closeness beta ^c	90	***	30 (26–34%)	71 (69–75%)	59 (55–64%)	64 (62–66%)
PLV betweenness gamma ^{b,c}	100	0.018	41 (39–46%)	79 (78–83%)	62 (60–67%)	71 (71–73%)
PLV degree gamma ^c	85	0.002	30 (26–33%)	66 (62–71%)	64 (55–70%)	65 (61–67%)
PLV eigenvector gamma ^{b,c}	90	0.011	38 (35–49%)	70 (68–81%)	68 (65–75%)	69 (68–75%)
MSI						
AEC alpha ^a	85	***	22 (18–28%)	59 (55–64%)	63 (56–70%)	61 (59–65%)
AEC degree delta ^a	65	0.004	23 (18–26%)	67 (61–70%)	56 (51–59%)	60 (58–62%)
PLV closeness broadband ^a	85	***	16 (13–21%)	59 (56–64%)	57 (54–61%)	58 (56–60%)
PLV betweenness gamma ^{a,b}	85	***	27 (22–36%)	65 (59–75%)	62 (57–69%)	63 (60–67%)
PLV closeness gamma ^a	85	***	26 (23–30%)	67 (64–71%)	60 (55–63%)	63 (61–65%)
AEC betweenness beta ^c	45	***	21 (18–25%)	66 (63–71%)	55 (51–58%)	60 (58–62%)
AEC degree beta ^{b,c}	90	0.028	31 (26–34%)	76 (71–79%)	56 (52–58%)	66 (63–67%)
AEC closeness gamma ^c	90	0.011	21 (18–27%)	64 (61–70%)	57 (54–60%)	60 (58–62%)
PLV closeness broadband ^c	95	0.016	16 (11–20%)	60 (57–66%)	55 (50–60%)	58 (55–60%)
PLV eigenvector delta ^c	85	0.012	33 (24–42%)	73 (68–83%)	59 (51–62%)	65 (61–68%)
PLV closeness beta ^c	90	***	24 (20–28%)	64 (60–69%)	60 (56–65%)	62 (60–64%)
PLV betweenness gamma ^{b,c}	90	***	35 (26–40%)	65 (57–76%)	69 (62–75%)	68 (65–71%)
PLV closeness gamma ^c	95	***	33 (29–40%)	65 (63–73%)	69 (62–71%)	68 (64–70%)

^aComputed on data with IEDs.^bFC measure that is both predictive of the EZ and the surgical outcome.^cComputed on data without IEDs.

***P-value < 0.001.

HD-EEG and MEG using graph-theory measures revealing the centrality of regions involved in causing seizures. Our findings showed that FC from iEEG and HD-EEG/MEG-VSs were predictive of outcome with PPV and NPV of 57–82% and 55–73% (validated using leave-one-out cross-validation, [Table 3](#)), respectively. Furthermore, these predictive network hubs (with FC values above or equal to their connectivity thresholds) had lower distance from resection in good- compared to poor-outcome patients. These hubs overlapped to resection in an average of 60% (range: 54–64%), 66% (range: 40–76%) and 70% (range: 50–82%) of good-outcome patients, for iEEG, HD-EEG-VSs and MEG-VSs, respectively. Our findings were also evident even at the patient's level: non-invasive FC measures were concordant with invasive ones despite being recorded at different times ([Fig. 3](#)). Moreover, resection of highly connected hubs was associated with seizure freedom. Contrarily, scattered areas of such hubs, which were not all resected, were associated with poor outcome. For example, in poor-outcome Patient 25 ([Fig. 3](#)), brain areas with high FC overlapped with the primary motor cortex that was preserved to avoid permanent motor deficits.

State of the art epilepsy surgery care involves using multiple data forms to formulate a treatment plan. Deactivation of the EZ is usually performed when several stereotyped seizures are recorded during long-term iEEG monitoring. Yet, interictal data can assist the decision-making, as for example, when no ictal activity is recorded. To assess the additive value of FC in the presurgical evaluation, we used the ECD as a comparative technique.⁶⁷ We tested whether surgical removal of regions where ECDs were located predicted outcome as FC did. We found that outcome prediction through FC (from iEEG and VSs) obtained better results compared to ECDs. Taken together, our findings highlight the additive value of our method in the non-invasive localization of highly connected hubs. Yet, our method is not intended to be used in isolation but rather in conjunction with existing techniques. Such methodology may augment the planning of iEEG placement by predicting, through non-invasive data, pathological hubs that should be recorded during long-term monitoring and hence minimizing the risk for insufficient coverage leading to surgical failure. It may also be beneficial in cases where the EZ overlaps eloquent areas preventing its complete resection. In these cases, the identification and disconnection of neighbouring pathological hubs (located outside eloquent areas) that are responsible for the early spread of seizure activity to the rest of the network may also lead to favourable outcome.

Limitations and future perspective

Despite its innovation, our study presents some limitations. Simultaneous MEG and HD-EEG recordings were performed at different times than iEEG, and thus this did not capture the exact same activity. Also, we did not take advantage of the full-head coverage that HD-EEG and MEG provide; instead, we constructed VSs at the locations of iEEG contacts. Moreover, we limit our analysis in frequencies up to 50 Hz. Future studies should use whole-brain VSs and include higher frequencies (up to 200 Hz) using sophisticated signal processing methods specifically tailored for the robust detection of high-frequency oscillations.^{68,69} To account for FC differences between HD-EEG and MEG, further investigations may use combined electromagnetic source imaging that provide a more complete reconstruction of the underlying generators.^{70,71} Our findings may also be considered in the context of patient-specific dynamical network models based on the principle of 'sources' and 'sinks'.⁷² Future studies may estimate source-sink

metrics from VSs time series extracted non-invasively from HD-EEG and MEG data to also validate their role as a non-invasive interictal biomarker of the EZ. Finally, our tool has the ability to reconstruct brain signals with similar FC features with those obtained invasively through iEEG. Thus, it can be applied to cohorts where iEEG cannot be obtained, such as in typically developing children, helping us to understand the concept of FC in healthy brain and how this change in pathology.

Conclusions

We reveal for the first time the non-invasive mapping of pathological hubs in the brain of children and young adults with DRE through the 'implantation' of VSs based on ESI/MSI. Non-invasive mapping of these hubs can predict surgical outcome better than conventional ESI/MSI. Our method may augment surgical planning by optimizing iEEG recordings and reducing surgical mortality. Most importantly, it may improve the outcome of patients with DRE undergoing surgery, particularly those who were previously ineligible for neurosurgery due to minimal or absent epileptiform activity in their electrophysiological recordings.

Funding

This work was supported by the National Institute of Neurological Disorders and Stroke (R01NS104116-01A1, Principal Investigator (PI): Christos Papadelis; and R21NS101373-01A1, PIs: Christos Papadelis and Steve M. Stuffelbeam).

Competing interests

The authors report no competing interests.

Supplementary material

[Supplementary material](#) is available at *Brain* online.

References

1. Aaberg KM, Gunnes N, Bakken IJ, et al. Incidence and prevalence of childhood epilepsy: A nationwide cohort study. *Pediatrics*. 2017;139:1-9.
2. Mohammadzadeh P, Nazarbaghi S. The prevalence of drug-resistant-epilepsy and its associated factors in patients with epilepsy. *Clin Neurol Neurosurg*. 2022;213:107086.
3. Oldham MS, Horn PS, Tsevat J, Standridge S. Costs and clinical outcomes of epilepsy surgery in children with drug-resistant epilepsy. *Pediatr Neurol*. 2015;53:216-220.
4. Baca CB, Vickrey BG, Caplan R, Vassar SD, Berg AT. Psychiatric and medical comorbidity and quality of life outcomes in childhood-onset epilepsy. *Pediatrics*. 2011;128:e1532e1543.
5. Berg AT. Epilepsy, cognition, and behavior: The clinical picture. *Epilepsia*. 2011;52(Suppl 1):7-12.
6. Xue-Ping W, Hai-Jiao W, Li-Na Z, Xu D, Ling L. Risk factors for drug-resistant epilepsy: A systematic review and meta-analysis. *Medicine (Baltimore)*. 2019;98:e16402.
7. Batchelor R, Taylor MD. Young adults with epilepsy: Relationships between psychosocial variables and anxiety, depression, and suicidality. *Epilepsy Behav*. 2021;118,107911:1-9.

8. Engel J. What can we do for people with drug-resistant epilepsy?: The 2016 Wartenberg lecture. *Neurology*. 2016;87:2483-2489.
9. Saada F, Wang ZS, Bautista RED. In focus: The everyday lives of families of adult individuals with epilepsy. *Epilepsy Behav*. 2015;50:10-13.
10. Dwivedi R, Ramanujam B, Chandra PS, et al. Surgery for drug-resistant epilepsy in children. *N Engl J Med*. 2017;377:1639-1647.
11. Willie JT, Laxpati NG, Drane DL, et al. Real-time magnetic resonance-guided stereotactic laser amygdalohippocampotomy for mesial temporal lobe epilepsy. *Neurosurgery*. 2014;74:569-585.
12. Duncan JS, Winston GP, Koepp MJ, Ourselin S. Brain imaging in the assessment for epilepsy surgery. *Lancet Neurol*. 2016;15:420-433.
13. Zijlmans M, Zweiphenning W, van Klink N. Changing concepts in presurgical assessment for epilepsy surgery. *Nat Rev Neurol*. 2019;15:594-606.
14. Stam CJ, Tewarie P, van Dellen E, van Straaten ECW, Hillebrand A, van Mieghem P. The trees and the forest: Characterization of complex brain networks with minimum spanning trees. *Int J Psychophysiol*. 2014;92:129-138.
15. Richardson MP. Large scale brain models of epilepsy: Dynamics meets connectomics. *J Neurol Neurosurg Psychiatry*. 2012;83:1238-1248.
16. Bettus G, Ranjeva JP, Wendling F, et al. Interictal functional connectivity of human epileptic networks assessed by intracerebral EEG and BOLD signal fluctuations. *PLoS One*. 2011;6:e20071.
17. Goodale SE, González HFJ, Johnson GW, et al. Resting-state SEEG may help localize epileptogenic brain regions. *Neurosurgery*. 2020;86:792-801.
18. Lagarde S, Roehri N, Lambert I, et al. Interictal stereotactic-EEG functional connectivity in refractory focal epilepsies. *Brain*. 2018;141:2966-2980.
19. Sinha N, Dauwels J, Kaiser M, et al. Predicting neurosurgical outcomes in focal epilepsy patients using computational modelling. *Brain*. 2017;140:319-332.
20. Shah P, Bernabei JM, Kini LG, et al. High interictal connectivity within the resection zone is associated with favorable post-surgical outcomes in focal epilepsy patients. *Neuroimage Clin*. 2019;23(April):101908.
21. Kini LG, Bernabei JM, Mikhail F, et al. Virtual resection predicts surgical outcome for drug-resistant epilepsy. *Brain*. 2019;142:3892-3905.
22. Millán AP, van Straaten ECW, Stam CJ, et al. Epidemic models characterize seizure propagation and the effects of epilepsy surgery in individualized brain networks based on MEG and invasive EEG recordings. *Sci Rep*. 2022;12:1-20.
23. Cardinale F, Rizzi M, Vignati E, et al. Stereoelectroencephalography: Retrospective analysis of 742 procedures in a single centre. *Brain*. 2019;142:2688-2704.
24. Önal Ç, Otsubo H, Araki T, et al. Complications of invasive subdural grid monitoring in children with epilepsy. *J Neurosurg*. 2003;98:1017-1026.
25. Nissen IA, Stam CJ, Reijneveld JC, et al. Identifying the epileptogenic zone in interictal resting-state MEG source-space networks. *Epilepsia*. 2017;58:137-148.
26. Juárez-Martínez EL, Nissen IA, Idema S, et al. Virtual localization of the seizure onset zone: Using non-invasive MEG virtual electrodes at stereo-EEG electrode locations in refractory epilepsy patients. *Neuroimage Clin*. 2018;19(May):758-766.
27. Cao M, Galvis D, Vogrin SJ, et al. Virtual intracranial EEG signals reconstructed from MEG with potential for epilepsy surgery. *Nat Commun*. 2022;13:1-12.
28. Wieser HG, Blume WT, Fish D, et al. ILAE Commission Report Proposal for a New Classification of Outcome with Respect to Epileptic Seizures Following Epilepsy Surgery Commission on Neurosurgery of the International League Against Epilepsy (ILAE) 1997–2001.
29. Oostenveld R, Praamstra P. The five percent electrode system for high-resolution EEG and ERP measurements. *Clin Neurophysiol*. 2001;112:713-719.
30. Tadel F, Baillet S, Mosher JC, Pantazis D, Leahy RM. Brainstorm: A user-friendly application for MEG/EEG analysis. *Comput Intell Neurosci*. 2011;2011:1-13.
31. de Macedo Rodrigues K, Ben-Avi E, Sliva DD, et al. A FreeSurfer-compliant consistent manual segmentation of infant brains spanning the 0–2 year age range. *Front Hum Neurosci*. 2015;9(FEB):1-12.
32. Tamilya E, Matarrese MAG, Ntolkeras G, et al. Noninvasive mapping of ripple onset predicts outcome in epilepsy surgery. *Ann Neurol*. 2021;89:911-925.
33. Matarrese MAG, Loppini A, Jahromi S, et al. Electric source imaging on intracranial EEG localizes spatiotemporal propagation of interictal spikes in children with epilepsy. *Annu Int Conf IEEE Eng Med Biol Soc*. 2021;2021:2668-2671.
34. Gramfort A, Papadopoulou T, Olivi E, Clerc M. OpenMEEG: Opensource software for quasistatic bioelectromagnetics. *Biomed Eng Online*. 2010;9:1-20.
35. van Veen BD, van Drongelen W, Yuchtman M, Suzuki A. Localization of brain electrical activity via linearly constrained minimum variance spatial filtering. *IEEE Trans Biomed Eng*. 1997;44:867-880.
36. Ricci L, Matarrese M, Peters JM, et al. Virtual implantation using conventional scalp EEG delineates seizure onset and predicts surgical outcome in children with epilepsy. *Clin Neurophysiol*. 2022;139:49-57.
37. Muthukumaraswamy SD. High-frequency brain activity and muscle artifacts in MEG/EEG: A review and recommendations. *Front Hum Neurosci*. 2013;7(MAR):1-11.
38. Papadelis C, AlHilani M, Pearl PL. Artifacts in pediatric and adult magnetoencephalography. In: Tatum W, ed. *Atlas of artifacts in clinical neurophysiology*. 2018:183-204.
39. Ramaraju S, Wang Y, Sinha N, et al. Removal of interictal MEG-derived network hubs is associated with postoperative seizure freedom. *Front Neurol*. 2020;11(September):1-9.
40. Chu CJ, Tanaka N, Diaz J, et al. EEG Functional connectivity is partially predicted by underlying white matter connectivity. *Neuroimage*. 2015;108:23-33.
41. van Dellen E, Douw L, Hillebrand A, et al. Epilepsy surgery outcome and functional network alterations in longitudinal MEG: A minimum spanning tree analysis. *Neuroimage*. 2014;86:354-363.
42. Wilke C, Worrell G, He B. Graph analysis of epileptogenic networks in human partial epilepsy. *Epilepsia*. 2011;52:84-93.
43. Bruns A, Eckhorn R, Jokeit H, Ebner A. Amplitude envelope correlation detects coupling among incoherent brain signals. *Neuroreport*. 2000;11:1509-1514.
44. Iandolo G, Chourasia N, Ntolkeras G, et al. Changes in the functional brain network of children undergoing repeated epilepsy surgery: An EEG source connectivity study. *Diagnostics (Basel)*. 2021;11:1234.
45. Lachaux JP, Rodriguez E, Martinerie J, Varela FJ. Measuring phase synchrony in brain signals. *Hum Brain Mapping*. 1999;8:194-208.
46. Colclough GL, Brookes MJ, Smith SM, Woolrich MW. A symmetric multivariate leakage correction for MEG connectomes. *Neuroimage*. 2015;117:439-448.

47. Englot DJ, Hinkley LB, Kort NS, et al. Global and regional functional connectivity maps of neural oscillations in focal epilepsy. *Brain*. 2015;138:2249–2262.
48. Saba V, Premi E, Cristillo V, et al. Brain connectivity and information-flow breakdown revealed by a minimum spanning tree-based analysis of MRI data in behavioral variant frontotemporal dementia. *Front Neurosci*. 2019;13(March):1–16.
49. Corona L, Tamilia E, Madsen JR, Stufflebeam SM, Pearl PL, Papadelis C. Mapping functional connectivity of epileptogenic networks through virtual implantation. *Annu Int Conf IEEE Eng Med Biol Soc*. 2021;2021:408–411.
50. Cabral J, Luckhoo H, Woolrich M, et al. Exploring mechanisms of spontaneous functional connectivity in MEG: How delayed network interactions lead to structured amplitude envelopes of band-pass filtered oscillations. *Neuroimage*. 2014;90:423–435.
51. Ghosh A, Rho Y, McIntosh AR, Kötter R, Jirsa VK. Noise during rest enables the exploration of the brain's dynamic repertoire. *PLoS Comput Biol*. 2008;4:e1000196.
52. Perinelli A, Tabarelli D, Miniussi C, Ricci L. Dependence of connectivity on geometric distance in brain networks. *Sci Rep*. 2019;9:1–9.
53. Castelluzzo M, Perinelli A, Tabarelli D, Ricci L. Dependence of connectivity on the logarithm of geometric distance in brain networks. *Front Physiol*. 2021;11:1868.
54. Tamilia E, AlHilani M, Tanaka N, et al. Assessing the localization accuracy and clinical utility of electric and magnetic source imaging in children with epilepsy. *Clin Neurophysiol*. 2019;130:491–504.
55. Alhilani M, Tamilia E, Ricci L, et al. Ictal and interictal source imaging on intracranial EEG predicts epilepsy surgery outcome in children with focal cortical dysplasia. *Clin Neurophysiol*. 2020;131:734–743.
56. Lüders HO, Najm I, Nair D, Widdess-Walsh P, Bingman W. The epileptogenic zone: General principles. *Epileptic Disord*. 2006;8(Suppl 2):S1–S9.
57. Jehi L. The epileptogenic zone: Concept and definition. *Epilepsy Curr*. 2018;18:12–16.
58. Tamilia E, Dirodi M, Alhilani M, et al. Scalp ripples as prognostic biomarkers of epileptogenicity in pediatric surgery. *Ann Clin Transl Neurol*. 2020;7:329–342.
59. Benjamini Y, Hochberg Y. Controlling the false discovery rate: A practical and powerful approach to multiple testing. *J R Stat Soc Ser B (Methodological)*. 1995;57:289–300.
60. Schober P, Schwarte LA. Correlation coefficients: Appropriate use and interpretation. *Anesth Analg*. 2018;126:1763–1768.
61. van Mierlo P, Carrette E, Hallez H, et al. Ictal-onset localization through connectivity analysis of intracranial EEG signals in patients with refractory epilepsy. *Epilepsia*. 2013;54:1409–1418.
62. van Diessen E, Hanemaaijer JI, Otte WM, et al. Are high frequency oscillations associated with altered network topology in partial epilepsy? *Neuroimage*. 2013;82:564–573.
63. Dimitriadis SI, Routley B, Linden DE, Singh KD. Reliability of static and dynamic network metrics in the resting-state: A MEG-beamformed connectivity analysis. *Front Neurosci*. 2018;12:1–22.
64. Aydin Ü, Pellegrino G, Ali Ob, et al. Magnetoencephalography resting state connectivity patterns as indicators of surgical outcome in epilepsy patients. *J Neural Eng*. 2020;17:035007.
65. Niso G, Carrasco S, Gudín M, Maestú F, Del-Pozo F, Pereda E. What graph theory actually tells us about resting state interictal MEG epileptic activity. *Neuroimage Clin*. 2015;8:503–515.
66. Hämäläinen M, Hari R, Ilmoniemi RJ, Knuutila J, Lounasmaa OV. Magnetoencephalography—Theory, instrumentation, and applications to noninvasive studies of the working human brain. *Rev Mod Phys*. 1993;65:413–497.
67. Laohathai C, Ebersole JS, Mosher JC, et al. Practical fundamentals of clinical MEG interpretation in epilepsy. *Front Neurol*. 2021;12(October):1–22.
68. Papadelis C, Tamilia E, Stufflebeam S, et al. Interictal high frequency oscillations detected with simultaneous magnetoencephalography and electroencephalography as biomarker of pediatric epilepsy. *J Vis Exp*. 2016;2016:54883.
69. Zhou Y, You J, Kumar U, et al. An approach for reliably identifying high-frequency oscillations and reducing false-positive detections. *Epilepsia Open*. 2022;7(4):674–686.
70. Aydin Ü, Vorwerk J, Dümpelmann M, et al. Combined EEG/MEG can outperform single modality EEG or MEG source reconstruction in presurgical epilepsy diagnosis. *PLoS One*. 2015;10:e0118753.
71. Plummer C, Vogrin SJ, Woods WP, Murphy MA, Cook MJ, Liley DTJ. Interictal and ictal source localization for epilepsy surgery using high-density EEG with MEG: A prospective long-term study. *Brain*. 2019;142:932–951.
72. Gunnarsdottir KM, Li A, Smith RJ, et al. Source–sink connectivity: A novel interictal EEG marker for seizure localization. *Brain*. 2022;145:3901–3915.